Research Square

Preprints are preliminary reports that have not undergone peer review.
They should not be considered conclusive, used to inform clinical practice,
or referenced by the media as validated information.

Evaluation of Brachystegia Eurycoma Leaves Extract as a Source of Green Inhibitor for Mild Steel in Acid Solution

L. N. Emembolu (ln.emembolu@unizik.edu.ng)
Nnamdi Azikiwe University Awka
F. U. Iwuchkwu
Nnamdi Azikiwe University Awka
C. C. Ejiofor
Nnamdi Azikiwe University Awka
J. J Ajali
Nnamdi Azikiwe University Awka

Article

Keywords: B. eurycoma leaf extract, green inhibitor, EIS, quantum chemical parameters, Simulations

Posted Date: September 12th, 2023

DOI: https://doi.org/10.21203/rs.3.rs-3323660/v1

License: This work is licensed under a Creative Commons Attribution 4.0 International License.
Read Full License

Additional Declarations: No competing interests reported.

EVALUATION OF B*RACHYSTEGIA EURYCOMA* LEAVES EXTRACT AS A SOURCE OF GREEN INHIBITOR FOR MILD STEEL IN ACID SOLUTION

L. N. Emembolu,[a,*] F. U. Iwuchkwu,[a] C.C. Ejiofor,[a] J.J Ajali[a,]**

[a] Department of Chemical Engineering, Nnamdi Azikiwe University Awka, Anambra state- Nigeria

Corresponding authors email: * ln.emembolu@unizik.edu.ng, https://orcid.org/0000-0001-5370-8107

** jj.ajali@unizik.edu.ng, https://orcid.org/0009-0003-6685-3081

Abstract

The aim of this work is to investigate the corrosion inhibition of *B. eurycoma* leaves extract as a natural inhibitor for mild steel corrosion in 1 M H2SO4 solution. The corrosion inhibition activity was analyzed by electrochemical impedance spectroscopy (EIS) and potentiodynamic polarization. The surface roughness and its properties through Scan electron microscopy (SEM). The obtained result from EIS divulge that the gradual increase in the *B. eurycoma* l eaves extract inhibitor concentration and time of immersion leads to progressive increase in inhibition efficiency. At the end of 8 hrs immersion time and inhibitor concentration of 1000mg/l the highest inhibition efficiency of (80%) and surface coverage of 70% were achieved. The potentiodynamic polarization results indicated that addition of *B. eurycoma* leaves extract hindered the reaction rates of anodic and cathodic reactions and performed as mix type inhibitor. The result also revealed that in the presence of *B. eurycoma* leaves extract the value of corrosion density of mild steel reduced considerably from 265.2μA/cm^2 for sample without inhibitor to 67.8μA/cm^2 for sample in 1000mg/l of the inhibitor. Again, it was observed that in the presence *B. eurycoma* leaves extract the mechanism of hydrogen (effervescence) evolution was unique whereas the anodic dissolution of iron mechanism experienced the impact of the inhibitor. SEM inspection revealed that the mild steel surface showed smoother and lower damage in the presence of inhibitor. Obvious correlations were found between corrosion inhibition efficiency and some quantum chemical parameters such as energy of highest occupied molecular orbital (E_{HOMO}), energy of lowest unoccupied molecular orbital (E_{LUMO}), energy gap ($E_{L–H}$) and electronic density etc. The obtained results were further elucidated with frontier molecular orbital theory.

KEYWORDS: *B. eurycoma* leaf extract, green inhibitor, EIS, quantum chemical parameters, Simulations

1. INTRODUCTION

The applicastion of mild steel in chemical industries cannot be overemphasized due to its mechanical characterization and wide range of applications like structural materials for pipelines, vessels and industrial tools that easily corrode when in contact with solvents [1, 2]. Most acid solutions used for cleaning, acid descaling metal etching and other acidic operations have potentials of causing damage to the metal surface, and the use of organic originated inhibitors has been reported as one of the greatest option amongst others for prevention of corrosion in metals

[1, 3, 4]. Hydrochloric acid, sulfuric acid and nitric acid are the most frequently used acids. The alloys of iron and iron are reactive materials with high potency of corroding in acidic solutions and inhibitor addition protects them from acid damages [5]. Generally, interactions between metals and the acidic medium in use exposed industrial facilities and equipment to corrosion thereby causing unfavorable economic implications [3]. The important characteristics of materials and structures like appearance, gas and liquid permeability & strength is downgraded by corrosion and hence reduces the material's utility efficiency [6]. As regards the current economy of the nation and financial burden caused by corrosion damages, several researchers has explored possible methods of improving metal resistance. Corrosion inhibitors are chemical compounds that decreases the rate of corrosion in a material when added to either liquids or gases [3, 6]. The efficiency of a corrosion inhibitor is dependent on factors like quantity of water, flow regime and the fluid composition. They could also be used as additives to fluids surrounding the metals [1, 6]. Inhibitors improves performance of materials and age of the equipment without altering the process technology [7]. Previous works done by researchers [16-19] on increasing the efficiency of organic compounds with hetero-atoms traces as corrosion inhibitors for mild steel in acidic medium was reported by [6]. In processes for corrosion prevention caused by free electron pairs, the contact between hetero-atoms like oxygen, nitrogen, phosphorus, sulphur and double/triple bond in the form of a wall and mild steel plays an important part. More so, as a result of the environmental damages caused by synthetic induced corrosion inhibitors, investigation of natural products from plant origin as corrosion inhibitors has greatly increased due to their ecofriendly and cost effective characteristics. The plant originated products are also biodegradable, nontoxic and renewable materials [8]. Ozoemena, Akpan [6] recorded several plant extracts like *Gliricidia sepium, Azadirachta indica, Pterocarpus soyauxii Taul, Momordica charantia and Boscia senegalensis* that has been initially explored as corrosion inhibitors. Recently, the effect of kalmegh leaf extract on the corrosion behavior of aluminum alloy in 1M NaOH solution was investigated using, potentiodynamic polarization, and electrochemical impedance spectroscopy (EIS) techniques. The results obtained showed that the inhibitor acts as a mixed type, controlling both the anodic and the cathodic reactions. Also, the maximum inhibition efficiency of 82.24 and 82.45% from EIS and PDP studies, respectively, were achieved at higher concentration by Namrata, et al, [20]. Equally**,** Onyenanu, etal, 2022, [26] worked on A. mossambicensis and E. sonchifolia Leaves' Extracts on Aluminium in Alkaline Media using Gravimetric and Electrochemical measurements obtained maximum inhibition efficiency of 79.04 and 77.00% each in KOH and NaOH respectively.

Brachystegia eurycoma (widely identified as Achi in the eastern part of Nigeria) widely grown in the tropical rain forest of West Africa. In Eastern part of Nigeria, the edible seed serves as a thickener in one of their famous local soups, functional agents in formulation of meats and in bakery products. Furthermore, the seed also possesses antimalarial, anti-inflammatory, anti-corrosion and anti-diabetics features. Computational methods have been used extensively in several fields using software development approach and visible in the use of quantum chemical calculations for corrosion studies [21-25]. The electronic and geometrical configuration of the inhibitor can easily be deduced by the application of quantum chemical calculations. In this study, the theoretical and experimental inhibition of mild steel by *Brachystegia eurycoma* extract in acidic environment was studied and researched. The surface morphology of steel samples in the

H_2SO_4 acidic solution was observed using scanning electron microscopy (SEM) and Fourier transform infrared (FTIR). Finally, density functional theory (DFT) calculation was used to analyze the effect of structural parameters on the efficiency of the inhibitors.

2. Materials and Method

2.1 Materials

Reagents used in the current work were obtained from Head Bridge Onitsha market without further treatment. The mild steel sheet was mechanically cut into coupons with dimensions 3cm x 8cm x 0.2cm. The coupons were polished with sand papers of different grades of coarseness from 200-1000, cleaned with distilled water, ethanol and then dried with dryer.

2.1.1 Collection and preparation of *B. eurycoma* leaves

B. eurycoma leaves used in this work was collected from a village called Ngene-Ugbo in Enugu State and identified in the Department of Botany, Nnamdi Azikiwe University Awka. The leaves were rinsed in distilled water thrice, sun dried for 48 hours and ground into powder. The *B. eurycoma* leaves extract was prepared by concentrating in a rotary evaporator after obtaining extract from Soxhlet extraction with 99% C_2H_5OH at 75 °C. The *B. eurycoma* leaves extract was stowed in 5^oC refrigerator and used as a corrosion inhibitor for steel in hydrochloric acid solutions. The functional groups of the *B. eurycoma* leaves extract was identified by FTIR analyzer.

2.1.2 Test solutions

The corrosion experiments were done in 1M H_2SO_4 solution in the absence and presence of various *B. eurycoma* concentrations. The 1 M H_2SO_4 solutions were prepared with concentrated H_2SO_4 solution and distilled water. The concentrations of the inhibitor were varied from 0.0 to 1.0 mg/l. Analytical-grade chemical reagents in distilled water without further purification were used in preparing all the test solutions. Freshly prepared solution was used for each experiment. The pressure and temperature of the experiments were controlled by opening the test solutions to the atmosphere and maintaining the temperature at 298k thermostatically.

2.1.3 Instrumental analysis

- Characterization of *B. eurycoma* leaves extract

The functional groups in major components of *B. eurycoma* leaves extract were examined using FTIR analyzer. Identification of the groups in organic components was done by Thermo Fisher Nico-let iS10 instrument within the range of 600 – 4567 cm^{-1} wave number and were shielded by *B. eurycoma* leaves extract respectively. On the other hand, the resistance related to charge transfer without and with *B. eurycoma* leaves extract were elucidated by R_{ct}^{0} and R_{ct}.

- Surface morphology examination

The inspection of surface morphology on the inhibited and uninhibited species were done in 1M HCl solution. Surface analysis was conducted by SEM model Philips XL30 microscope. Analysis of contact angle were carried out by utilizing OCA 15 plus type system.

2.2 Methods

2.2.1 **Electrochemical measurements**

EIS and Potentiodynamic polarization measurements were done by employing GILL AC attached to a software known as "gill". The fitting and associated parameters were obtained through Zview software package. All experiments were done in a cell with three electrode configuration: MS as working, Ag/AgCl (3 M KCl) as reference and platinum sheet with 2 cm^2 surface area as the counter electrodes. The working electrode was immersed in test solution for 30 min to a establish steady state open circuit potential (Eocp). After measuring the Eocp, the electrochemical measurements were performed. The polarization measurements were done by scanning the potential in the range of –250 to +250mV at $1mVs^{-1}$. The EIS results were obtained over a frequency range between 0.01Hz and 10 kHz with 10mV amplitude. The Eqs. (1) and (2) were used for the calculation of the corrosion inhibition efficiency based on polarization ($\eta_{polarization}$) and EIS (η_{EIS}) results[27]:

$$\eta_{polarization} = \left(1 - \frac{i_{corr}}{i^{\circ}_{corr}}\right) \times 100 \quad (1)$$

$$\eta_{EIS} = \left(1 - \frac{R^{\circ}_{ct}}{R_{ct}}\right) \times 100 \quad (2)$$

Where the i^{0}_{corr} and i_{corr} is the corrosion current densities of the samples subjected to the H_2S0_4 solution and the electrolyte protected by *B. eurycoma* leaves extract, respectively. Similarly, the

parameters of R^0_{ct} and R_{ct} is the resistance related to charge transfer without and with *B. eurycoma* leaves extract.

2.2.2 Quantum studies

Theoretical calculations were performed with Gaussian 03, E.01, and software. The electron/atoms calculations of inhibitor molecules were conducted by the density functional theory (DFT)/B3LYP method [12]. Analysis of information about molecular geometric and electron distributions as well as inhibitor efficiencies and inhibitor−surface inter- actions due to its accuracy and less time requirement from the computational point of view was validated with DFT [27-28]. All the geometric variables without any symmetry constraints for the geometries of all studied inhibitors were optimized. On other hand, no imaginary frequency was recorded after Frequency calculation indicating the existence of minimum-energy structures. Hence, the application of Koopman's theorem (1, 3) was useful in evaluating the electronic properties such as electron affinity (A) and ionization potential (I) because it provides relationship between the electron affinity, the ionization potential and the energies (ie the energy of highest occupied molecular orbital E_{HOMO}, energy of the lowest unoccupied molecular orbital E_{LUMO}), highest occupied molecular orbital HOMO, and the lowest unoccupied molecular orbital LUMO and ($\Delta E_{L\text{-}H} = E_{LUMO} - E_{HOMO}$) correspondingly. Furthermore, A and I are related to E_{HOMO} and the E_{LUMO} as shown in the Eqs. (3) and (4) below; [12, 29 -31] [9].

$$I = -E_{HOMO} \tag{3}$$

$$A = -E_{LUMO} \tag{4}$$

The absolute hardness, η, and absolute electronegativity, χ, of the inhibitor molecule were calculated as;

$$\chi = \frac{I+A}{2} = -\frac{E_{HOMO}+E_{LUMO}}{2} \tag{5}$$

$$\eta = \frac{I-A}{2} = \frac{E_{LUMO}-E_{HOMO}}{2} = \frac{1}{2}\Delta E_{L-H} \tag{6}$$

The global softness, σ, can also be defined as follows:

$$\sigma = \frac{1}{\eta} \tag{7}$$

$$N = \frac{-\chi_{inhibitor}}{2\eta_{inhibitor}} \tag{8}$$

The fraction of electrons transferred from the inhibitor molecule to the metallic atom (ΔN) was calculated according to Pearson from the obtained values of χ and η. For the calculation the following formula was used:

$$\Delta N = \frac{\phi - \chi_{inhibitor}}{2\eta_{inhibitor}} = \frac{\chi_{Fe} - \chi_{inhibitor}}{2(\eta_{Fe} + \eta_{inhibitor})} \tag{9}$$

Using a theoretical value in Eq. (11) the work function of iron (ϕ) was substituted with its electronegativity χ_{Fe} = 7eV and a global hardness of $\eta_{Fe} = zero$, by assuming that for a metallic bulk I = A, because they are softer than the neutral metallic atoms [9][40]. Additionally, DFT code Dmol^3 were utilized in studying the nucleophilic and electrophilic performance of the chosen inhibitor spices by considering the atom- condensed Fukui indices resulting from the local reactivity of the green inhibiting compounds.

2.2.3. **Molecular simulations.**

Molecular dynamic (MD) simulations as an efficient and reliable technique have been utilized in this work to elucidate the experimental findings, and throw more light on the existence of thermonuclear adsorption of the *B. eurycoma* leaves extract (components) on the metal substrate.

Forcite molecular dynamics was employed to calculate different energy of adsorption configurations of molecule on Fe surface. The Fe surface was cleaved along the (110) plane because it has a density packed surface and the most stabilization at this position. Calculations were carried out in a 12 x 10 super cell using the COMPASS (Condensed phase optimized molecular potentials for atomistic simulation studies) force field and the smart algorithm with NVT canonical ensemble, a time step of 1fs, and simulation time 5000 ps is in line with [32-33]. The interactions and binding energies of the *B. eurycoma* leaves inhibitor with the Fe (110) surface in the simulation system, were assessed using the following Eq. [31]:

$$E_{interaction} = E_{total} - \left(E_{surface + solution} + E_{inhibitor}\right) \tag{10}$$

$$E_{binding} = -E_{interaction} \tag{11}$$

where $E_{surface + solution}$ is assigned to the total energy of Fe (1 1 0) surface and solution without the inhibitors; $E_{inhibitor}$ indicate the total energy of inhibitors and E_{total} represents the total energy of the whole system.

3. Results and Discussions

3.1 Electrochemical measurements

The special effects of *B. eurycoma* leaves extract concentration on inhibition of mild steel was investigated by electrochemical impedance spectroscopy and potential dynamic polarization methods.

The impedance parameters between MS-tetraoxosulphate VI acid interface in the absence and presence of optimal concentration of *B. eurycoma* leaves extract was determined by EIS and the results obtained are presented in Table 1. The Open circuit potential (OCP), as a function of time for *B. eurycoma* leaves extract are presented in Fig. 1. It can be seen clearly from Fig.1 that increase in the concentrations of *B. eurycoma* leaves extract and immersion time caused gradual shift of OCP to extra negative values. It equally observable that the highest negative OCP values occurred in MS coupons immersed in 1M H_2S0_4 containing 200mg/L of *B. eurycoma* leaves extract for 8hrs. The obtained results can be attributed to the adsorption of inhibitors molecules on the MS surface which resulted in shift of OCP to extra negative values.

Fig. 1: OCP as a function of time for MS coupons immersed in 1M H_2SO_4 with and without different concentrations of *B. eurycoma* leaves extract.

Nyquist, bode and phase angle plots of MS coupons in 1 M H_2SO_4 solution in the presence and absence of different concentrations of *B. eurycoma* leaves extract are presented in Fig. 2(a–c) comprising of a semicircle shape known as Nyquist plots. Inspection of Fig. 2a shows that the electrochemical behavior of the blank solution was constant over time. It is evident from the obtained results that the entire plots are governed by only one time constant which implies that

the corrosion reaction is regulated by charge transfer. Furthermore, the shapes of the curves remains identical despite progressive increase or decrease in different concentrations of *B. eurycoma* leaves extract in 1 M H_2SO_4 solution. This shows that the mechanism were not affected by variations in concentrations of *B. eurycoma* leaves extract. Again, the diameter of Nyquist plots increases by increasing both the inhibitors concentration and the immersion time which can be attributed to the existence of adsorbed organic compounds from *B. eurycoma* leaves extract on mild steel surface thereby consolidating the formation of the inhibitive film. Modeling of the impedance plots and extraction of electrochemical parameters was done with one-time constant electrical equivalent circuit (R(RQ)). The models employed are solution resistance (R_s), total resistance (R_t), (R_t = charge transfer resistance (Rct) + inhibitor film resistance (R_f)) and constant phase element (CPE_t) respectively. Hence, the Double layer capacitance (C_t) data was evaluated using Eq. (12); [34-36].

$$C_t = \frac{(R_t \times Y_0)^{\frac{1}{n}}}{R_t} \qquad (12)$$

Where Y_0 = proportionality constant, R_t = total resistance, $n = {}^{\tau}/_{(\pi/2)}$ and that τ is the phase angle of CPE. "n" is fractional exponent for solid electrodes/solution interfaces and its value is $-1 \leq n \leq 1$ (Chaitra et al., 2016). Depending on the value of n, CPE can represent resistance (n = 0, Y_o = R), capacitance (n = 1, Y_o = C), inductance (n = -1, Y_O = L) [37-38].

Table 1 shows that increase in the concentrations of *B. eurycoma* leaves extract increases the value of R_t. Also, increase in immersion time leads to increase in low frequency impendence ($|Z|_{10\,mHz}$) and R_t values in the presence of different concentrations of *B. eurycoma* leaves extract. Similarly, the maximum high frequency angle($\theta_{10\,kHz}$), ($|Z|_{10\,mHz}$) and R_t were achieved in the presence of 1000mg/L *B. eurycoma* leaves extract depicting the high surface coverage of adsorbed inhibitor molecules. Deductions from Table 1 presents gradual increase in "n" which resulted from increase in the concentrations of *B. eurycoma* leaves extract and immersion time. This can be as a result of decline in the surface roughness and inhomogeneity caused by adsorption of inhibitor molecules [39-41]. Table 1 points out that increase in phase angle resulted from increase in the inhibitor concentration and this is as a result of reduction in surface irregularities due to adsorption of organic molecules *B. eurycoma* leaves extract on the Mild steel [42-43].

Here, it is noteworthy that the gradual increase in the inhibitor concentration and immersion time resulted in the substantial decrease of double layer capacitance which leads to increase in the protective film thickness and causing a decrease in the dielectric constant. Fig. 2(b) shows Bode plots have a solitary peak indicating that electrochemical impedance measurements is appropriate for one time constant equivalent model. Furthermore, Fig. 2(c), presents a substantial increase in phase angle value compared to the blank solution which is attributable to capacitive response of adsorption of the inhibitor molecules on the metal surface.

Table 1: Data for electrochemical parameters estimated from modeling impendence of mild steel in H_2SO_4 solution in the absence and present of *B. eurycoma* leaves extract

It equally observable from Table 1, increase in the inhibitors concentration and immersion time causes a substantial decrease in the values of double layer capacitance implying that the reduction in dielectric constant is due to the replacement of water molecules with the inhibitor molecules. [42-43]. The potentiodynamic polarization studies was done by determining the consequences of *B. eurycoma* leaves extract on the cathodic hydrogen ions reduction reaction and anodic dissolution of mild steel in H_2SO_4 solution. The polarization is presented in Fig 3. The values of corrosion potential, $E_{corr,}$ corrosion density, $i_{corr,}$ cathodic Tafel, β_c, and anodic Tafel, $\beta_{a,}$ slopes were obtained with the help of linear Tafel extrapolation and presented in Table 2. Close examination of Table 2, reveals that increase in *B. eurycoma* leaves extract in H_2SO_4 solution caused substantial rise in corrosion density, i_{corr} and small change of $E_{corr,}$ to additional negative values. The maximum value obtained in displacing E_{corr} is 50mV at 1000mg/L which is less than 85mV implying that the rise in inhibitor shifted E_{corr} to more negative values but the shift is not substantial and as a result the type of inhibitor either anodic or cathodic cannot be determine[34,38,44]. The obtained results simply indicates that increase in the inhibitor concentration caused both anodic and cathodic branches to move towards lower current densities. This shows that *B. eurycoma* leaves extract performed as a mixed type inhibitor. Also, it is observable from Fig. 3, that in the presence of *B. eurycoma* leaves extract the anodic Tafel slope decreased substantial while the cathodic Tafel slope appeared constant.

Fig 2: Impedance spectra of mild steel in H_2SO_4 solution in the absence and presence of *B. eurycoma* leaves extract.

This can be attributed to the fact that, the adsorption of inhibitors molecules on the metal surface did not alter the mechanism of hydrogen evolution rather the anodic mechanism of iron dissolution was altered. Also, it depicts that the adsorption of inhibitors on the anodic lively spot followed chemisorption process while on that of cathodic lively spot the inhibitors presented mainly physical impediments towards the aggressive ions [21,43,45]

Table 2: Polarization parameters of mild steel in HCl in the presence and absence of B.*eurycoma* leaves extract.

Fig 3. Potentiodynamic polarization curves for mild steel in H_2SO_4 in the presence and absence of different concentration of B.*eurycoma* leaves extracts.

The inhibition efficiency (η%) and surface coverage (θ%) were obtained using Eqs. (13) and (14) respectively [14, 40]

$$\eta\% = 100\left(1 - \frac{R_{t,b}}{R_{t,i}}\right) \tag{13}$$

$$\theta\% = 100\left(1 - \frac{C_{t,i}}{C_{t,b}}\right) \tag{14}$$

Where "b" and "i" represents blank and inhibited solutions respectively.

Inspection of Fig. 4 below shows that increase in exposure time results in increase of inhibition efficiency and surface coverage respectively which can be an attribute of adherence of the inhibitor molecules on the lively spot of the mild steel. Based on existing literature, [46-47], *B. eurycoma* leaves extracts contains some vital organic compounds. These inhibitor molecules adsorb on the lively spot of mild steel through chemical adsorption known as chemisorption or physical adsorption called physiorption. According to Fig 4, the highest inhibition efficiency of *B. eurycoma* leaves extracts is 85% which can be attributed to the interaction of the π- electron cloud

Fig 4: Plot of surface coverage and inhibition efficiency with respect to time.

of the donor atoms or lone pairs of electrons of oxygen atoms with the vacant d-orbital of the mild steel. It is also noteworthy from literature that natural inhibitors or green corrosion inhibitors accounts for up to 80-96 percent inhibition efficiency and as such *B. eurycoma* leaves extract with 85% inhibition efficiency can be considered as a good and active green corrosion inhibitor of mild steel in H_2SO_4 solution. Investigation of adsorption isotherms shows that Langmuir adsorption isotherm Fig 5 best describes the adsorption of *B. eurycoma* leaves extracts on mild steel in H_2SO_4 with $R^2 > 0.99$. Also, (Eq.15) gives mathematical expression of Langmuir adsorption isotherms as: [27]

$$\frac{C_{inh}}{\theta} = \frac{1}{K_{ads}} + C_{inh} \quad (15)$$

Where, θ, k_{ads} and C refers to the degree of surface coverage on the metal surface, equilibrium constant and inhibitor concentration respectively.

Fig 5: Plot of Langmuir adsorption isotherm fitted on impedance value of mild steel in H_2SO_4 containing different concentrations of *B. eurycoma* leaves extract.

3.2 Surface characterizations

3.2.1 FTIR analysis

Close examination of Fig. 6a reveals that the functional groups (O–H, C=O, C=N or C–O), of *B. eurycoma* leaves extracts contain oxygen and nitrogen which is the backbone of corrosion inhibitors. The corrosion products on the mild steel surface immersed in 1 M H_2SO_4 containing 1000 mg L^{-1} of inhibitor as seen on FTIR spectrum of Fig 6b has the absorption peaks of O–H, C=O/C=N, C–N, C–O–C which appeared at 3432 cm^{-1}, 1632 cm^{-1}, 1390 cm^{-1}, 1126 cm^{-1} correspondingly.

Fig 6: FTIR spectra of (a) natural *B. eurycoma* leaves extracts and (b) *B. eurycoma* leaves extracts film adsorbed on the mild steel surface.

These observations can be accredited to the adherence of *B. eurycoma* leaves extracts on the mild steel surface. Again, looking at Fig 6a the band width of 3428 cm^{-1} with a broader curvature which is attributable to the existence of molecular interactions was ascribed to the O–H stretching vibrations. Noticeable stretching vibration of C–H seen at 2931 cm^{-1} was accredited to C=O/C=N bending. The occurrence of absorption peaks at 1388 cm^{-1} and 1058 cm^{-1} can be attributed to stretching vibrations of C–N in the amides and C–O groups respectively [28].

3.2.2 SEM Inspection

Further insight was gained on the inhibitory properties of *B. eurycoma* leaves extracts by analyzing the surface morphology of mild steel with scan electron microscopy SEM. The SEM micrographs of mild steel surface after 8h in 1 M H_2SO_4 in the absence and presence of 1000g L^{-1} of *B. eurycoma* leaves extracts were shown in Fig. 7. Critical inspection of Fig. 7b revealed profound gorges and big pits on the surface of mild steel in the absence of *B. eurycoma* leaves extracts, which differs greatly from the polished surface Fig. 7a. This can be attributed to the grave damage on the mild steel in 1 M H_2SO_4 solution. Although, it was clearly seen in Fig. 7c that the mild steel surface wears comparatively smoother morphology with 1000 mg L^{-1} *B. eurycoma* leaves extracts, which was identical to the polished surface. Additionally, the above occurrence suggests that the inhibitor molecules were adsorbed on the surface of mild steel to form a protecting film, which hindered the resulting corrosion from the aggressive solution to reach the surface of the metal. Therefore, the inhibitor glowingly shielded the mild steel from H2S04 attack.

Fig. 7: SEM micrographs of mild steel (a) polished, (b) after immersion without and (c) with 1000 mg/l of *B. eurycoma* leaves extracts, in 1 M H_2SO_4

3.3 Quantum calculations and Simulations mechanism considerations

Experimental findings were further investigated theoretically to ensure the existence of the adsorption of green inhibitors and their anticorrosion properties on the mild steel substrate under a different conditions, by adopting MD simulations as active and reliable approach. Table 3 shows the energetic features of *B. eurycoma* leaves extracts. Fig 8 presents the side view of the snapshot from molecular dynamics model. It is observed from the configuration (Fig 8) that each dissolved molecule of the green inhibitor adhered to the surface of Fe (110). This theoretical result implies that there is the propensity of the inhibitor to form protective film on the mild steel substrates. Again, as can be seen from the top and side view snapshots that the molecular backbone of the surface-bound inhibitor depicts a flat– lying adsorption orientation with regard to the iron surface. This orientation increases contact with inhibitor and as a result significant increase in the degree of surface coverage and corrosion resistant properties of the inhibitor constituents studied. However, the properties calculated by quantum chemical approach, give information about reactivity of these molecules but the reactivity cannot directly be translated to corrosion inhibition efficiency, which involves more processes such as competitive adsorption, film formation, etc. The adsorption energy (E_{ads}) which is important in characterizing the adsorption of these molecules onto the Fe surface was estimated using the Eq. (16)

$$E_{ads} = E_{total} - \left(E_{inhibitor} - E_{surface}\right) \quad (16)$$

where $E_{inhibitor}$, $E_{surface}$, and E_{total} represents the energy of a single molecule of these selected active components, the Fe slab without adsorption, and the total energy of the system containing a molecule and Fe surface, respectively. The negative values of adsorption energies indicate the adherence of inhibitive compounds onto the metallic (110) substrate.

Table 3: The energetic descriptors and outputs of *B. eurycoma* leaves extracts over Fe 110

It is well known from the electronic point of view that the adherence of corrosion inhibitors onto metallic surfaces is based on the donor –acceptor interaction [47-51]. Under such adsorption mechanism, the electron-rich centers of the inhibitors such as aromatic rings and oxygen heteroatoms donate their electrons to the vacant d orbitals of Fe atoms. Simultaneously, the inhibitor atoms can accept electrons from the filled orbitals of Fe atoms. Also, according to the frontier molecular orbital theory, it is evident that transfer of electronic charge which occur at inhibitor/metal interface is reliant on the highest occupied molecular orbital (HOMO) and lowest unoccupied molecular orbital (LUMO). The utmost ability of inhibitor to donate electrons through its energetic spot is depicted by HOMO whereas the LUMO presents the areas that accept electrons from HOMO of the metal cations Fig 8. Further calculations on the electron/atoms of the inhibitor molecules were done with the density functional theory DFT/B3LYP method [52 -55] to clarify more on HOMO and LUMO as well as the geometrics of *B. eurycoma* inhibitor. It is possible from Fig. 8 that the HOMO can be traced closely to the benzene ring and its adjoining methoxy group and carbonyl oxygen and C=C double bonds, whereas on the other hand the LUMO occurs on the carbon atoms of aromatic rings and the energetic carbonyl spots. Since there is the presence of methoxy in conjunction with carbonyl oxygen centers, aromatic benzene rings as well as the double bonds of C=C, these can donate their electrons to the void d orbitals of the surface Fe atoms, and as result interact with the surface metal cation by mechanism of donor-acceptor process. This can be attributed to the fact that the HOMO electrons are seen above the aromatic circles or

rings and on the carbonyl O atoms suggesting that the inhibitor can part with some of its delocalized π electron of aromatic circles and electron pairs of oxygenated energetic spots to vacant orbitals in the surface of metal cations. Again, investigation of the inhibitor geometry indicate that the HOMO orbital were dispensed above the circles and nearly on hydroxyl oxygen but the LUMO appeared on the middle circles. As evidenced in the Homo of DFT/B3LYP, the species can be found on the carbonyl bond and its surrounding cycle comprising of C=C double bonds, which implies donation of elections from the sensitive lively spots. Additionally, the pictorial view of HOMO and LUMO of *B. eurycoma* substance, it is obvious that the electron-rich benzene ring, C=C double bond as well as oxygen heteroatoms performed as the sensitive areas for HOMO thereby presenting their strong propensity for transferring of electrons to the surface of metal cation. Also, Fig. 8 shows the Electronic properties of N-methyl-3,4 methylenediOxy phenylpropan-3-amine which is a major component of *B. eurycoma* substance.

The global reactivity indices was elucidated via some inherent quantum chemical parameters which include energetics of molecular orbitals (ie E_{L-H} gap, E_{LUMO} and E_{HOMO}), electronic affinity, ionization potential, electronegativity, hardness and fracture of electronic charge transferred between the metal surface and the natural inhibitor etc were considered and the calculated values are presented in Table 4. The existing literature evidenced the widely acceptance that the small negative HOMO energy provide more charges to the vacant d orbitals of surface Fe cations. This is an indication that reduced energy gap (E_{L-H}) provides development to strengthen charge sharing at the interface of inhibitor and metal which leads to intensified interactions [52-54].

Table 4: Calculated quantum chemical parameters from DFT/B3LYP

Furthermore, Fukui indices for electrophilic and nucleophilic performance for the studied inhibitor was analyzed by considering the sensitive (reactive) energetic spot of the *B. eurycoma* inhibitor in acidic medium and presented in Fig. 8. It is observable from the Fig. 8 that the C=C double bond, aromatic circles, and carbonyl oxygen as well as methoxy presented electrophilic behavior corresponding to HOMO results thereby confirming the propensity to donate electron to the surface of Fe atoms with unfilled d orbitals [55-58]. Then, the carbonyl group, the carbon atoms above the circles and those in the double bond depicts nucleophilic behavior. Like the molecular orbital distribution the carbonyl O atoms, benzene ring as well as the hetrocyclic atoms performed as energetic spot for adsorption through electrophilic style thereby replicating their ability to provide electrons to the surface Fe cations, on the other hand, the ring carbon atoms acts as nucleophilic areas. Geometrically, it is possible that the minimum energy of acid inhibitor behaving in a nucleophilic manner can occur on hydroxyl O atom, while another hydroxyl oxygen and carbon atoms in close proximity acts like an energetic spots for nucleophilic attack of the inhibitor leading to donor- acceptor interactions due to the acceptance of electrons from filled orbital surface metal atoms [53-55]. Inspection of Fukui indices for electrophilic behavior of *B. eurycoma* inhibitor indicate that corrosion inhibition occurred between the heterocyclic O atom and aromatic rings or circles. This validates the HOMO results which is an indicative of the inhibitor binding to the surface of Fe (110) due delocalization of π electrons from lone pair electrons and aromatic rings to vacant d orbitals.

Fig 8: Electronic properties of N-methyl-3,4 methylenediOxy phenylpropan-3-amine

(a) Electron density, (b) electrophilic f (-), (c) nucleophilic f (+), (d) HOMO, (e) LUMO (f) side view of the snapshot for N-methyl-3,4 methylenedioxy phenylpropan-3-amine from molecular dynamics model. (g) top view of the Snapshot for N-methyl-3,4 methylenedioxy phenylpropan-3-amine from molecular dynamics model. Atom legend: white = H; gray = C; red = O. The blue and yellow isosurfaces depict the electron density difference: the blue regions show electron accumulation while the yellow regions show electron loss.

Conclusion

The corrosion inhibition properties of *B. eurycoma* leaves extract on corrosion mitigation of mild steel in 1M H2SO4 was carried via electrochemical, surface and quantum techniques. The obtained data divulge that organic inhibitors are present in B. eurycoma leaves extract. The inhibitor positively adhered on the mild steel surface and inhibited the corrosion rate. Increase in the inhibitor concentration and time leads to increase in surface coverage and inhibition efficiency. *B. eurycoma* leaves extract impressively diminished the corrosion current density thereby working as mixed type inhibitor. The hydrogen effervescence mechanism was not affected rather the mechanism of Fe dissolution. Surface examination, shows that surface roughness of mild steel was low in the presence of B. eurycoma leaves extract than in blank H2SO4. The contact angle inspection points to reduction of surface hydrophilicity as a result of adherence of organic inhibitors energetic spots of mild steel. The computational studies affirms that inhibitive compounds present in the natural B. eurycoma leaves extract adhered to the mild steel surface.

Competing interests

The authors declare non-financial interest with any organization.

Data availability statement

All data generated or analyzed during this study are included in this manuscript.

REFERENCE

1. Ozoemena, C., M. Charles, and M.C. Ugwuoke, Experimental and Theoretical Studies on the Corrosion Inhibitive Properties of mild Steel in 2M H2SO4 Acid Solution by Ethanolic Extract of Brachystegia Eurycoma Seed. Asian Journal of Science and Technology, 2019. **10**(12): p. 10532-10544.

2. Zida A., B.J., Kabré I., Sawadogo M.P., Sangaré I., Bamba S., Yacouba A., Ouédraogo A., Yonli D., Drabo F., et al., Epidemiological and clinical aspects of urogenital schistosomiasis in women, in Burkina Faso, West Africa. . Infect. Dis.Poverty 5:81. doi: 10.1186/s40249-016-0174-1., 2016.

3. Ozoemena, C.P. and M. Charles, Computational modeling and statistical analysis on the corrosion inhibition of aluminium in nitric acid solution by ethanolic extract of citrus sinesis seed. Global Journal of Pure and Applied Chemistry Research, 2019. **7**(1): p. 25-46.

4. Ahamad, I., R. Prasad, and M. Quraishi, Inhibition of mild steel corrosion in acid solution by Pheniramine drug: Experimental and theoretical study. Corrosion science, 2010. **52**(9), 3033-3041.

5. Ishtiaque Ahamad, R.P., Quraishi, M.A., Inhibition of mild steel corrosion in acid solution by Pheniramine drug: Experimental and theoretical study, Corrosion Science, 52 (2010) 3033–3041

6. Ozoemena, C.P., G.J. Akpan, and M.C. Ugwuoke, Corrosion inhibition and adsorption characteristics of ethanolic extract of brachystegia eurycoma seed on the corrosion of mild steel in 1M H_2SO_4 acid solution.

7. Adiba A. Mahmmod, Ivan A. Kazarinov, Anees A. Khadom and Hameed B. Mahood, Experimental and Theoretical Studies of Mild Steel Corrosion Inhibition in Phosphoric Acid Using Tetrazoles Derivatives. Journal of Bio- and Tribo-Corrosion (2018) 4:58.

8. Boudjellal et al., Experimental and theoretical approach to the corrosion inhibition of mild steel in acid medium by a newly synthesized pyrazole carbothioamide heterocycle. Journal of Molecular Structure, 2019

[9] Emembolu L. N., Igbokwe P.K., (2020), Inhibition Capability of *Dennettia Tripetala* Leaves Extract on Low Carbon Steel in 4 M HCL Solutions, Journal of Basic and Applied Research International, 26(1), 23-35

[10] Ali Döner, Ramazan Solmaz, Muzaffer Özcan, Gülfeza Kardas, (2011), Experimental and theoretical studies of thiazoles as corrosion inhibitors for mild steel in sulphuric acid solution, corrosion science, 53, 2902–2913. doi:10.1016/j.corsci.2011.05.027

[11] Ali Dehghani, Ghasem Bahlakeh, Bahram Ramezanzadeh,,Mohammad Ramezanzadeh, (2019), A combined experimental and theoretical study of green corrosion inhibition of mild steel in HCl solution by aqueous Citrullus lanatus fruit (CLF) extract, Journal of Molecular Liquids, https://doi.org/10.1016/j.molliq.2019.02.010

[12] Jia Jun Fu, HaiShan Zang, Ying Wang, SuNing Li, Tao Chen, and Xiao Dong Liu, (2012), Experimental and Theoretical Study on the Inhibition Performances of Quinoxaline and Its Derivatives for the Corrosion of Mild Steel in Hydrochloric Acid, American Chemical Society, 6377-6386

[13] Chris O. Akalezi, Emeka E. Oguzie, (2016), Evaluation of anticorrosion properties of Chrysophyllum albidum leaves extract for mild steel protection in acidic media, Int J Ind Chem, 7, 81–92. DOI 10.1007/s40090-015-0057-5

[14] Eiman, et al, (2018), Glycyrrhiza glabra leaves extract as a green corrosion inhibitor for mild steel in 1 M hydrochloric acid solution: experimental, molecular dynamics, Monte Carlo and quantum mechanics study. J Mol Liq 255:185–198, https://doi.org/10.1016/j.molliq.2018.01.144

[15] Turuvekere K. Chaitra, Kikkeri N. Mohana & Harmesh C. Tandon, (2018), Evaluation of newly synthesized hydrazones as mild steel corrosion inhibitors by adsorption, electrochemical, quantum chemical and morphological studies, Arab Journal of Basic and Applied Sciences, 25:2, 45-55, DOI: 10.1080/25765299.2018.1449347

[16] Olofinjana Sikemi, Oyebamiji Abel Kolawole, and Semire Banjo, (2017), Quantum Chemical Studies on Corrosion Inhibition of 1, 3-Thiazine Derivatives for Mild Steel in Acidic Media: DFT Approach, Manila Journal of Science 10, 44-63

[17] Sam John, et al, (2017), Corrosion inhibition properties of 1, 2, 4-Hetrocyclic Systems: Electrochemical, theoretical and Monte Carlo simulation studies, Eyptian iournal of petroleum, 26(3), 721-732. https://doi.org/10.1016/j.ejpe.2016.10.005

[18] Tsoeunyane M.G., Makhatha, M.E. and Arotiba O.A., (2019) Corrosion Inhibition of Mild Steel by Poly(butylene succinate)-L-histidine Extended with 1,6-diisocynatohexane Polymer Composite in 1 M HCl, International Journal of Corrosion, Article ID 7406409, https://doi.org/10.1155/2019/7406409

[19] El-Shamy A. M., El-Hadek M. A., Nassef, A. E. and El-Bindary R. A., (2020),

Optimization of the Influencing Variables on the Corrosion Property of Steel Alloy 4130 in 3.5 wt.% NaCl Solution, Journal of Chemistry, Article ID 9212491. https://doi.org/10.1155/2020/9212491

[20] Namrata et al (2017), Electrochemical approach of Kalmegh leaf extract on the corrosion behavior of aluminium alloy in alkaline solution, International journal of Industrial Chemistry 8:75-82.

[21] Barbouchi, etal, (2023), Theoretical and Experimental Studies of Lentisk Leaf Extract as Green Corrosion Inhibitor for Iron in Chloride Media, biointerface research in applied chemistry, Volume 13(6), https://doi.org/10.33263/BRIAC136.557

[22] Hsissou, etal, (2021), et al. Insight into the corrosion inhibition of novel macromolecular epoxy resin as highly efficient inhibitor for carbon steel in acidic mediums: Synthesis, characterization, electrochemical techniques, AFM/UV–Visible and computational investigations. J. Mol. Liq. 337, https://doi.org/10.1016/j.molliq.2021.116492.

[23] Udhayakala P., Rajendiran, T. V. & Gunasekaran, S., (2012), Theoretical approach to the corrosion inhibition efficiency of some pyrimidine derivatives using DFT method. Journal of Computational Methods in Molecular Design, 2 (1), 1-15.

[24] Verma, C. B., Ebenso, E. E., Bahadur, I., Obot, I. B., & Quraishi, M. A. (2015). 5-(Phenylthio)-3H-pyrrole-4-carbonitriles as effective corrosion inhibitors for mild steel in 1 M HCl: Experimental and theoretical investigation. Journal of Molecular Liquids, 212, 209–218. https://doi. org/10.1016/j.molliq.2015.09.009

[25] Verma, C. B., Singh, P., & Quraishi, M. A. (2016). A thermodynamical, electrochemical and surface investigation of Bis (indolyl) methanes as Green corrosion inhibitors for mild steel in 1 M hydrochloric acid solution. Journal of the Association of Arab Universities for Basic and Applied Sciences, 21, 24 –30. doi:10.1016/j.jaubas.2015.04.003

[26] C.N. Onyenanu, L. N. Emembolu, C.C. Ejiofor, (2022), Corrosion Inhibition potentials of *A. mossambicensis* and *E. sonchifolia* Leaves' Extracts on Aluminuium in Alkaline Media: Insights from Gravimetric and Electrochemical Studies, Chemistry Africa. https://doi.org /10.1007/s42250-022-00531-0

[27] Manh, et al, (2022), Corrosion Inhibition of Mild Steel in Hydrochloric Acid Environments Containing Sonneratia caseolaris Leaf Extract ACS Omega, 8874-8886. https://doi.org/10.1021/acsomega.1c07237

[28] Dongyi Li, Panpan Zhang, Xinyu Guo, Xiaowei Zhao and Ying Xu, (2019), The inhibition of mild steel corrosion in 1 M H_2SO_4 solution by radish leaf extract, *RSC Adv.*, (9), 40997-41009. DOI: 10.1039/C9RA04218K

[29] Bahlakah, et al, (2017), Experimental and theoretical studies of the synergistic inhibition effects between the plant leaves extract (PLE) and zinc salt (ZS) in corrosion control of carbon steel in chloride solution, Journal of molecular liquids, 248, 845-870 https://doi.org/10.1016/j.molliq.2017.10.120

[30] Loveth N. Emembolu, Chukwunonso O. Aniagor, Josiah C. Umembamalu, Chukwunonso N. Onyenanu, (2021), Electrochemical and statistical study of the inhibition effect of T. conophorum leaf extract on aluminum corrosion in acidic medium, Safety in Extreme Environments. https://doi.org/10.1007/s42797-021-00040-2**.**

[31] Hammud, et al, (2022), An Integrated Experimental and Theoretical Studies on the Corrosion Inhibition of Carbon Steel by Harmal Extracts, *Molecules 27*(21), 7250; https://doi.org/10.3390/molecules27217250

[32] Ojha, L.K., Tüzün, B. & Bhawsar, J. (2020), Experimental and Theoretical Study of Effect of *Allium sativum* Extracts as Corrosion Inhibitor on Mild Steel in 1 M HCl Medium. *J Bio Tribo Corros,* 39(6), https://doi.org/10.1007/s40735-020-00336-z

[33] Rajesh Haldhar, Dwarika Prasad, Akhil Saxena, Raman Kumar, (2018), Experimental and theoretical studies of Ficus religiosa as green corrosion inhibitor for mild steel in 0.5 M H2SO4 solution, Sustainable Chemistry and Pharmacy, 9, 95-105, https://doi.org/10.1016/j.scp.2018.07.002.

[34] Saviour Umoren, et al, (**2014),** Experimental and Theoretical Studies of Red Apple Fruit Extract as Green Corrosion Inhibitor for Mild Steel in HCl Solution, Journal of Dispersion Science and Technology, **789-802,** https://doi.org/10.1080/01932691.2014.922887

[35] L. N., Emembolu, Onukwuli, O. D., Umembamalu, C. J. and Aniagor, C. O., (2020), Evaluation of the corrosion inhibitory effect of *Napoleonaea imperalis* leaf extract on mild steel in 1.3 M H2SO4 medium, Journal of Bio- and Tribo- corrosion, 6(128), 1-15. https://doi.org/10.1007/s40735-020-00422-2

[36] Shehata**,** et al, (2022), Crispy Dry Chili Extract as an Eco-Friendly Corrosion Inhibitor for Mild Steel in Chloride Solutions: Experimental and Theoretical Studies, *Journal of Bio- and Tribo-Corrosion***,** 8(97)**,** https://doi.org/10.1007/s40735-022-00691-z

[37] Amrita Biswas, Sagar Pal, G. Udayabhanu, (2015), Experimental and theoretical studies of xanthan gum and its graft co-polymer as corrosion inhibitor for mild steel in 15% HCl, Applied Surface Science, 353, 173-183, https://doi.org/10.1016/j.apsusc.2015.06.128.

[38] Emori, et al, (2020), Adsorption and corrosion inhibition performance of multi-phytoconstituents from Dioscorea septemloba on carbon steel in acidic media: Characterization, experimental and theoretical studies, Colloids and Surfaces A: Physicochemical and Engineering Aspects, 590,124-534, https://doi.org/10.1016/j.colsurfa.2020.124534.

[39] Liu, et al, (2018), Corrosion protection for mild steel by extract from the waste of lychee fruit in HCl solution: Experimental and theoretical studies, Journal of Colloid and Interface Science, 520, 41-49. https://doi.org/10.1016/j.jcis.2018.02.071.

[40]. Rajesh Haldhar, Dwarika Prasad, Akhil Saxena and Priyanka Singh, (2018), *Valeriana wallichii* root extract as a green & sustainable corrosion inhibitor for mild steel in acidic environments: experimental and theoretical study**,** *Mater. Chem. Front.*, 2, 1225-1237, DOI: 10.1039/C8QM00120K

[41]. Vorobyova, V., Skiba, M., (2021), Peach Pomace Extract as Novel Cost-Effective and High-Performance Green Inhibitor for Mild Steel Corrosion in NaCl Solution: Experimental and Theoretical Research, *Waste Biomass Valor*, 12, 4623–4641. https://doi.org/10.1007/s12649-020-01333-6

[42]. Hui Cang, Zhenghao Fei, Wenyan Shi, Qi Xu, (2012), Experimental and Theoretical Study for Corrosion Inhibition of Mild Steel by L-Cysteine, International Journal of Electrochemical Science, 7(10), 10121-10131, https://doi.org/10.1016/S1452-3981(23)16263-8.

[43]. Yaxu Wu, Yuanmi Zhang, Yumiao Jiang, Yafeng Qian, Xugeng Guo, Li Wang, Jinglai Zhang, (2020), Orange peel extracts as biodegradable corrosion inhibitor for magnesium alloy in NaCl solution: Experimental and theoretical studies, Journal of the Taiwan Institute of Chemical Engineers, 115, 35-46, https://doi.org/10.1016/j.jtice.2020.10.010.

[44]. Daniel, E.F., Ebeagwu, M.C., Okafor, P.C. *et al.*, (2021), Exploring the Efficacy of Phytoconstituents from *Vernonia amygdalina* on Mild Steel Protection in Acid Environment: Combined Experimental and Theoretical Study, *J Bio Tribo Corros.,* 7(126), https://doi.org/10.1007/s40735-021-00562-z

[45]. Haldhar, R., Prasad, D. & Bhardwaj, N., (2020), Experimental and Theoretical Evaluation of *Acacia catechu* Extract as a Natural, Economical and Effective Corrosion Inhibitor for Mild Steel in an Acidic Environment, *J Bio Tribo Corros.,* 6(76) , https://doi.org/10.1007/s40735-020-00368-5

[46]. Liu Li Liao, Shi Mo, Hong Qun Luo, Nian Bing Li, (2017), Longan seed and peel as environmentally friendly corrosion inhibitor for mild steel in acid solution: Experimental and theoretical studies, Journal of Colloid and Interface Science, 499, 110-119, https://doi.org/10.1016/j.jcis.2017.03.091.

[47]. Al-Amiery, A.A., Mohamad, A.B., Kadhum, A.A.H. *et al.*, (2022), Experimental and theoretical study on the corrosion inhibition of mild steel by nonanedioic acid derivative in hydrochloric acid solution. *Sci Rep,* 12, 4705, https://doi.org/10.1038/s41598-022-08146-8

[48]. Olasehinde, E.F., Agbaffa, E.B., Adebayo, M.A. *et al.* (2022), Corrosion Inhibition of Mild Steel in 1 M HCl by Methanolic *Chromolaena odorata* Leaf Extract: Experimental and Theoretical Studies, *J Bio Tribo Corros,* 8, 105. https://doi.org/10.1007/s40735-022-00704-x

[49]. Anupama, K.K., Joseph, A. E(2018), xperimental and Theoretical Studies on *Cinnamomum verum* Leaf Extract and One of Its Major Components, Eugenol as Environmentally Benign Corrosion Inhibitors for Mild Steel in Acid Media, *J Bio Tribo Corros*, 4, 30 https://doi.org/10.1007/s40735-018-0146-z

[50]. Emembolu L. N., Igbokwe P.K., (2020), Inhibition capability of *Dennettia tripetala* leaves extract on low carbon steel in 4 M HCL solutions, Journal of basic and applied research international, 26(1), 23-35

[51]. Deyab M.A., Q. Mohsen, Lei Guo, (2022), Aesculus hippocastanum seeds extract as eco-friendly corrosion inhibitor for desalination plants: Experimental and theoretical studies, Journal of Molecular Liquids, 361,119594, https://doi.org/10.1016/j.molliq.2022.119594.

[52]. Cheng Xu, Bochuan Tan, Shengtao Zhang, Wenpo Li, (2022), Corrosion inhibition of copper in sulfuric acid by Leonurus japonicus Houtt. extract as a green corrosion inhibitor: Combination of experimental and theoretical research, Journal of the Taiwan Institute of Chemical Engineers, 139,104532, https://doi.org/10.1016/j.jtice.2022.104532.

[53]. Jeeja Rani A.T., Asha Thomas, Abraham Joseph, (2021), Inhibition of mild steel corrosion in HCl using aqueous and alcoholic extracts of Crotalaria Pallida – A combination of experimental, simulation and theoretical studies, Journal of Molecular Liquids, 334,116515, https://doi.org/10.1016/j.molliq.2021.116515.

[54]. Zerroug, et al, (2021), Experimental and theoretical evaluation of the adsorption process of some polyphenols and their corrosion inhibitory properties on mild steel in acidic media, Journal of Environmental Chemical Engineering, 9(6), 106482, https://doi.org/10.1016/j.jece.2021.106482.

[55]. Rajesh Haldhar, Dwarika Prasad, Akhil Saxena, (2018), Armoracia rusticana as sustainable and eco-friendly corrosion inhibitor for mild steel in 0.5M sulphuric acid: Experimental and theoretical investigations, Journal of Environmental Chemical Engineering, 6(4), 5230-5238, https://doi.org/10.1016/j.jece.2018.08.025.

[56]. Nor etal, (2020), Environmentally conscience corrosion inhibitors for mild steel in corrosive hydrochloric acid solution by *Uncaria Cordata* extract: experimental and theoretical studies, Journal of Adhesion Science and Technology, https://doi.org/10.1080/01694243.2023.2196905

[57]. Anis etal, (2023), Experimental and theoretical study of polysaccharides extracted from prickly pear nopales Pulp (PPUN) of Opuntia ficus-indica as corrosion inhibitors, Journal of Molecular Liquids, 384, 122272, https://doi.org/10.1016/j.molliq.2023.122272.

[58]. Sadegh Pour-Ali, Reza Tavangar, Seyedsina Hejazi, (2023), Comprehensive assessment of some l-amino acids as eco-friendly corrosion inhibitors for mild steel in HCl: Insights from experimental and theoretical studies, Journal of Physics and Chemistry of Solids, 181, 111550, https://doi.org/10.1016/j.jpcs.2023.111550.

TABLES

Table 1: Data for electrochemical parameters estimated from modeling impendence of mild steel in H_2SO_4 solution in the absence and present of *B. eurycoma* leaves extract

System	Immersion Time (hr)	R_t (Ωcm^2)	$Y_{0,t}$ ($\mu s^n \Omega^{-1} cm^{-2}$)	n_t	C_t ($\mu F cm^{-2}$)	τ (ms)	Log|Z| (Ωcm^2)	Phase angle (^{o})
Blank	2	133	177	0.78	67.3	8.3	2.4	1.4
200mg/L B	6	346	52.8	0.89	33	12	2.5	14.2
1000mg/L B	10	1263	34.1	0.90	20.2	16	2.9	25.3

Table 2: Polarization parameters of mild steel in HCl in the presence and absence of B.*eurycoma* leaves extract.

Solution	E_{corr} vs SCE (mV)	i_{corr} ($\mu A/cm^2$)	β_a (V/dec)	- β_c (V/dec)
Blank	-605.6 ± 37.1	265.2 ± 3.1	0.8 ± 0.03	0.2 ± 0.02
200mg./L	-652.3 ± 35.1	67.8 ± 0.2	0.25 ± 0.02	0.1 ± 0.01
1000mg/L	-758.4 ± 33.6	48.0 ± 0.1	0.3 ± 0.01	0.1 ± 0.01

Table 3: The energetic descriptors and outputs of *B. eurycoma* leaves extracts over Fe 110

Descriptors (kcal/mol)	Outputs
Total energy	-330.447
Adsorption energy	-199.332
Rigid adsorption energy	-197.848
Deformation energy	-1.822
dE_{ads}/dN_i	-199.332

Table 4: Calculated quantum chemical parameters from DFT/B3LYP

Inhibitor	E_H	E_L	ΔE_{L-H}	A	I	χ	η	ΔN
B. eurycoma	-6.860	-2.810	4.080	2.810	6.860	4.835	1.858	0.540

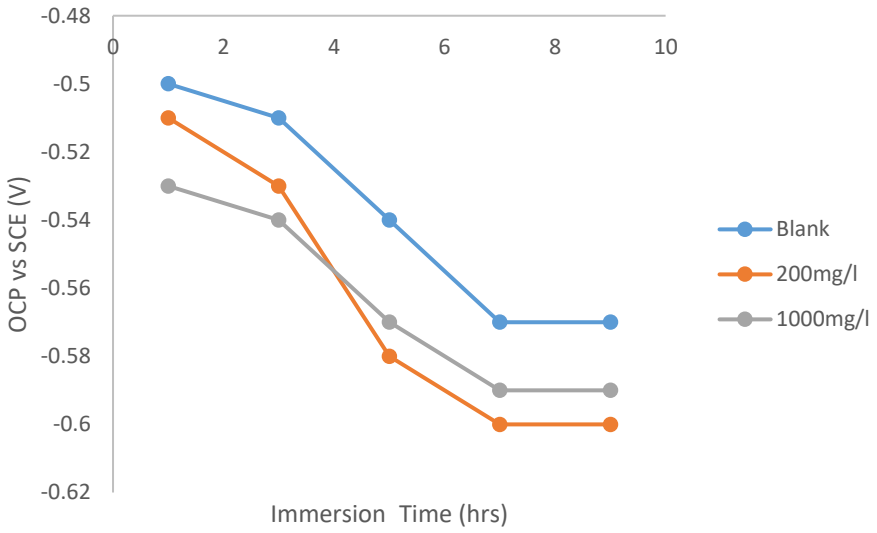


Fig. 1: OCP as a function of time for MS coupons immersed in 1M H_2SO_4 with and without different concentrations of *B. eurycoma* leaves extract.

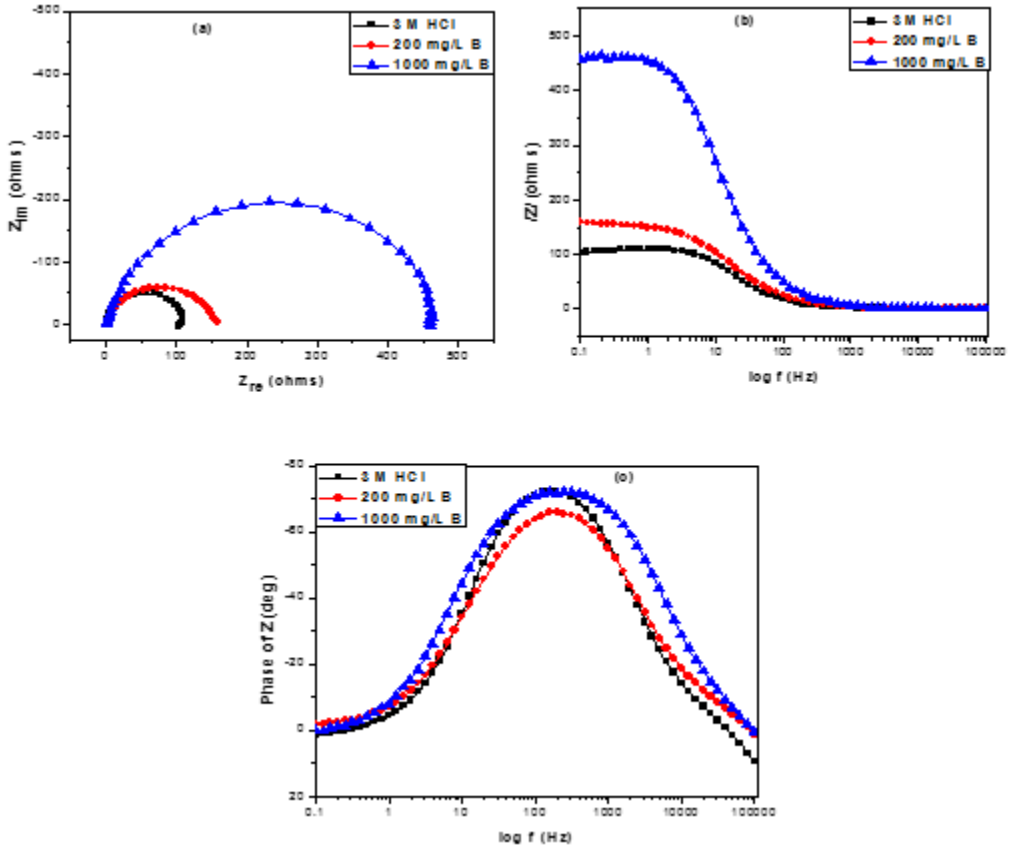


Fig 2: Impedance spectra of mild steel in H_2SO_4 solution in the absence and presence of *B. eurycoma* leaves extract.

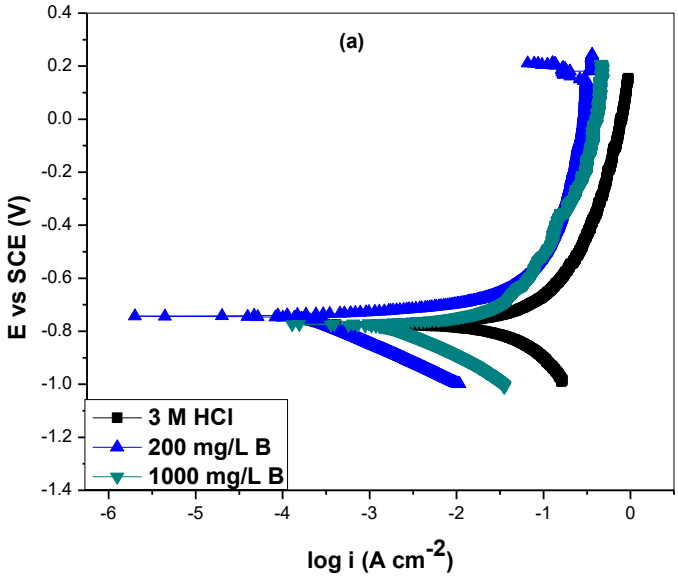


Fig 3. Potentiodynamic polarization curves for mild steel in H_2SO_4 in the presence and absence of different concentration of B.*eurycoma* leaves extracts.

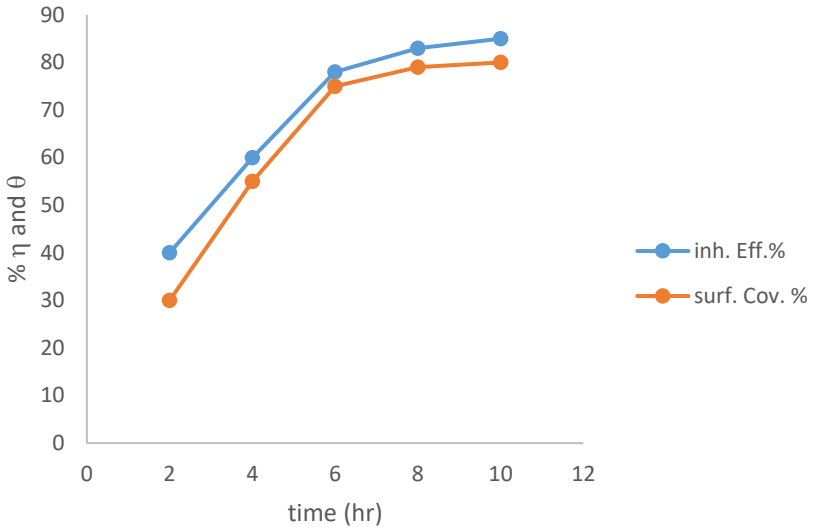


Fig 4: Plot of surface coverage and inhibition efficiency with respect to time.

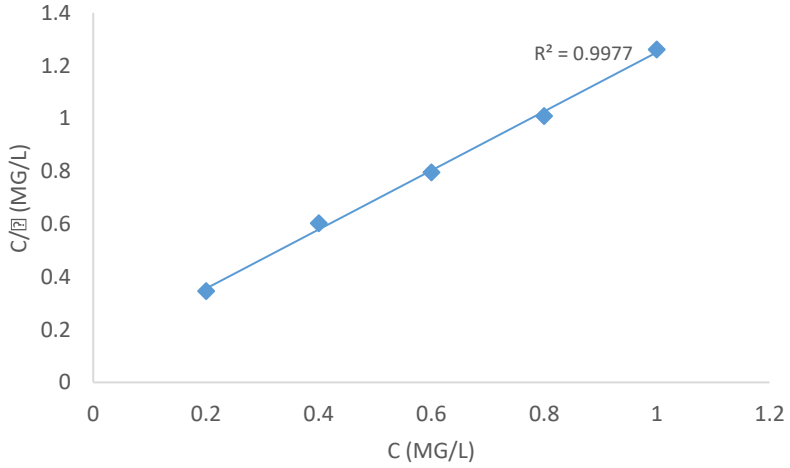


Fig 5: Plot of Langmuir adsorption isotherm fitted on impedance value of mild steel in H_2SO_4 containing different concentrations of *B. eurycoma* leaves extract.

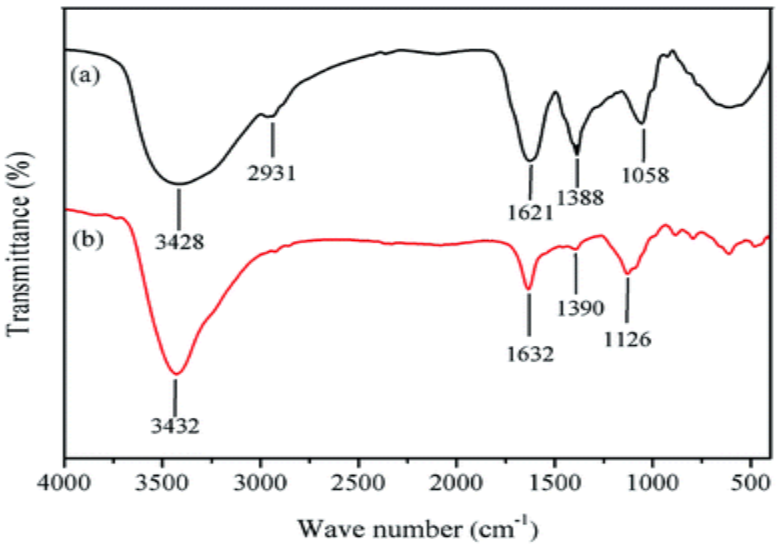


Fig 6: FTIR spectra of (a) natural *B. eurycoma* leaves extracts and (b) *B. eurycoma* leaves extracts film adsorbed on the mild steel surface.

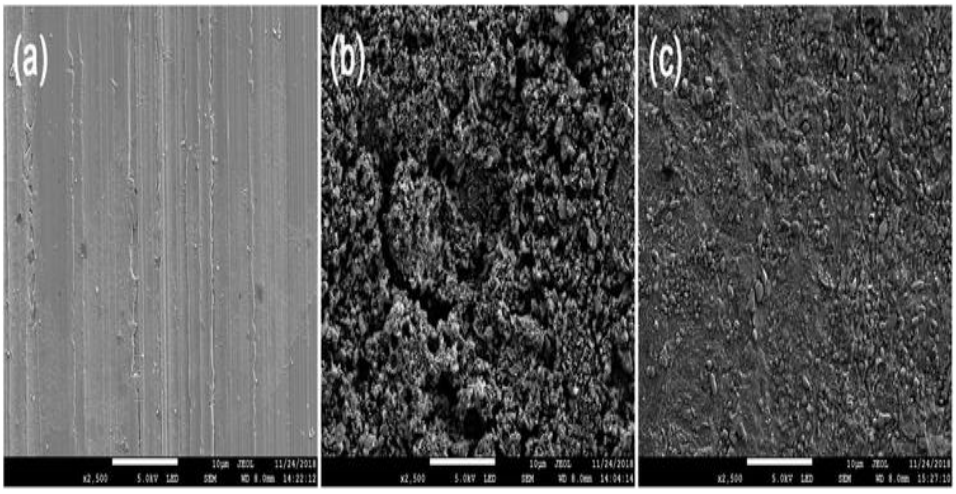


Fig. 7: SEM micrographs of mild steel (a) polished, (b) after immersion without and (c) with 1000 mg/l of *B. eurycoma* leaves extracts, in 1 M H_2SO_4

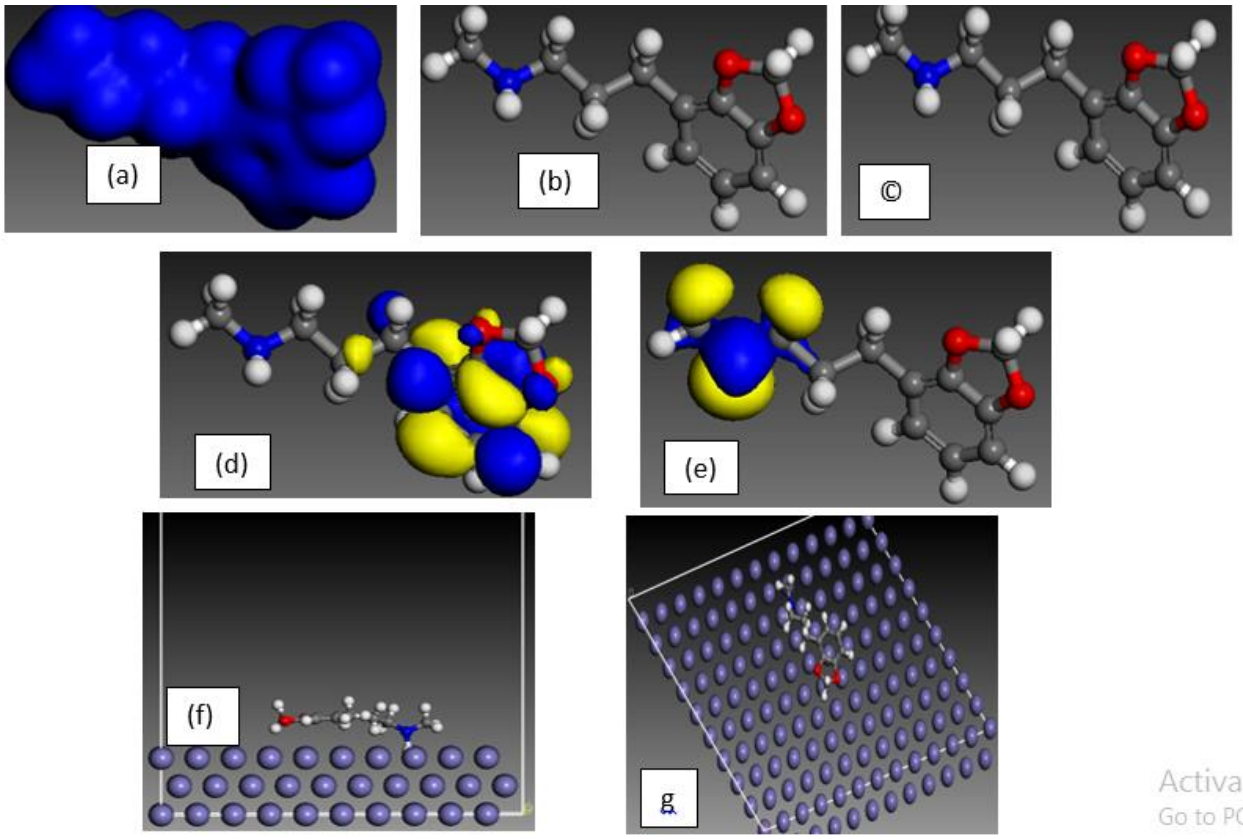


Fig 8: Electronic properties of N-methyl-3,4 methylenediOxy phenylpropan-3-amine

(a) Electron density, (b) electrophilic f (-), (c) nucleophilic f (+), (d) HOMO, (e) LUMO (f) side view of the snapshot for N-methyl-3,4 methylenedioxy phenylpropan-3-amine from molecular dynamics model. (g) top view of the Snapshot for N-methyl-3,4 methylenedioxy phenylpropan-3-amine from molecular dynamics model. Atom legend: white = H; gray = C; red = O. The blue and yellow isosurfaces depict the electron density difference: the blue regions show electron accumulation while the yellow regions show electron loss.